Materials Today Physics 45 (2024) 101463

Contents lists available at ScienceDirect

Materials Today Physics

journal homepage: www.journals.elsevier.com/materials-today-physics

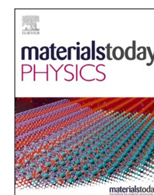

Engineering shallow and deep level defects in κ-Ga_2O_3 thin films: comparing metal-organic vapour phase epitaxy to molecular beam epitaxy and the effect of annealing treatments

P. Mazzolini [a,b,*], J.B. Varley [c], A. Parisini [a], A. Sacchi [a], M. Pavesi [a], A. Bosio [a], M. Bosi [b], L. Seravalli [b], B.M. Janzen [e], M.N. Marggraf [e], N. Bernhardt [e], M.R. Wagner [f,e], A. Ardenghi [f], O. Bierwagen [f], A. Falkenstein [d], J. Kler [d], R.A. De Souza [d], M. Martin [d], F. Mezzadri [g,b], C. Borelli [a], R. Fornari [a,b]

[a] Department of Mathematical, Physical and Computer Sciences, University of Parma, Viale delle Scienze 7/A, 43124 Parma, Italy
[b] IMEM-CNR, Viale delle Scienze 37/A, 43124 Parma, Italy
[c] Lawrence Livermore National Laboratory, Livermore, United States
[d] Institute of Physical Chemistry, RWTH Aachen University, D-52056 Aachen, Germany
[e] Technische Universität Berlin, Institute of Solid State Physics, Hardenbergstr. 36, 10623 Berlin, Germany
[f] Paul-Drude-Institut für Festkörperelektronik, Leibniz-Institut im Forschungsverbund Berlin e.V., Hausvogteiplatz 5-7, 10117 Berlin, Germany
[g] Department of Chemistry, Life Sciences and Environmental Sustainability, University of Parma, Viale delle Scienze 17/A, 43124 Parma, Italy

ABSTRACT

Orthorhombic gallium oxide (κ-Ga_2O_3) is an ultra-wide bandgap semiconductor with great potential in new generation electronics. Its application is hindered at present by the limited physical understanding of the relationship between synthesis and functional properties. This work discusses the effects of growth method (metal-organic vapour phase epitaxy and molecular beam epitaxy) as well as annealing treatments in different atmospheres (O_2, H_2) on point defects in κ-Ga_2O_3 layers epitaxially grown on c-plane sapphire. Comprehensive experimental characterization by X-ray diffraction, photo current-as well as photoluminescence excitation spectroscopy, and X-ray photo electron spectroscopy is combined with first principles calculations of the point defects' formation and complex-dissociation energies. We demonstrate that for κ-Ga_2O_3 the concentration of shallow and deep level defects can be sensitively controlled through annealing treatments at temperatures (T = 500 °C) well below the thermal stability threshold of this polymorph. In particular, our results suggest that hydrogen-related defects (*e.g.*, H-interstitials, Ga-vacancies—H complexes) play a key role in this process. While we provide direct exemplary implications of our results for the performances of κ-Ga_2O_3 based photodetectors, these findings are predicted to impact further application fields of κ-Ga_2O_3, such as high electron mobility transistors or memory devices.

Gallium oxide is an ultra-wide bandgap ($E_g \approx 5$ eV) semiconductor that possesses five different polymorphs, *i.e.,* β, κ (also referred as ε) [1], α, γ [2], and δ [3]. Its most investigated polytype is the thermodynamically stable β-Ga_2O_3. For this polymorph, the possibility to grow the material from the melt [4] and to control its electrical properties over a wide range through extrinsic doping [5] opened up to its possible application in different fields, *e.g.* power electronics [6,7], UVC-photodetection [8–10]. Nonetheless, metastable Ga_2O_3 polymorphs are gaining increasing attention. In particular, the hexagonal α and the orthorhombic κ are the most promising alternatives to β because of their higher symmetry crystal structure which can be more easily accommodated on relatively cheap substrates (*e.g.,* sapphire, MgO) for the realization of multi-layer heterostructures [11]. Moreover, κ-Ga_2O_3 possesses a large spontaneous polarization along the [001] direction [12–17] with a suggested switchable behaviour (*i.e.*, ferroelectric properties) [18], it shows the possibility to tune its bandgap through In- and Al-alloying [19,20], and it is suggested to have a large dielectric constant [21]. The combination of these characteristics are very appealing for application fields spanning from high electron mobility transistors (HEMT) [22,23] to non-volatile memory devices [15,16,24], and quantum-well infrared photodetectors [25] with properly designed heterostructures. Nonetheless, achieving a fine control over the relationship between synthesis and functional properties in κ-Ga_2O_3 has still to be achieved. In this framework, the presence of vertically-oriented structural defects in (001) κ-Ga_2O_3 epitaxial layers (*e.g.*, rotational domains) is an issue [26], and their reduction [27,28] / suppression [29]

* Corresponding author.
E-mail address: piero.mazzolini@unipr.it (P. Mazzolini).

https://doi.org/10.1016/j.mtphys.2024.101463
Received 4 March 2024; Received in revised form 3 May 2024; Accepted 14 May 2024
Available online 15 May 2024
2542-5293/© 2024 The Authors. Published by Elsevier Ltd. This is an open access article under the CC BY license (http://creativecommons.org/licenses/by/4.0/).

are important milestones for this material system. On the other hand, only limited theoretical and experimental efforts have been devoted to the investigation and control of point defects in κ-Ga_2O_3 [26,30]. These aspects are currently hindering its widespread application for the most technologically demanding fields. In contrast, in simpler resistive solar-blind UVC-photodetector (PD) devices, nominally undoped κ-Ga_2O_3 layers on c-plane sapphire substrates are already showing promising performance, compatible with the state of the art of the most investigated β polymorph [31–33].

In this work we study the effect of mild annealing treatments in different background atmospheres on (001) κ-Ga_2O_3 epitaxial layers deposited by metal organic vapour phase epitaxy (MOVPE) and by molecular beam epitaxy (MBE) on c-plane sapphire substrates. Based on *(i)* the combination of various experimental techniques (time-of-flight secondary ion mass spectrometry ToF-SIMS, X-ray photoelectron spectroscopy XPS, photoluminescence spectroscopy PL and photoluminescence excitation spectroscopy PLE), *(ii)* the fabrication/characterization of PDs, and *(iii)* theoretical calculations with density functional theory (DFT), we investigate the formation of different point defects and the dissociation of defect complexes in κ-Ga_2O_3. In particular, the interpretation of our results points strongly toward H-related defects being mostly responsible for the detected changes in the performances of κ-Ga_2O_3-based PDs upon mild thermal treatments. Similarly to what has been already demonstrated in the case of β-Ga_2O_3 [34–38], we here provide unprecedented experimental and theoretical evidence that also in the κ polymorph hydrogen plays a fundamental role to determine its functional properties, being able to act as a shallow (interstitial H_i, oxygen substitutional H_O) donor as well as a deep (Ga vacancies V_{Ga}-H complexes) acceptor defect. In particular, an O_2 annealing treatment is found to significantly improve the PD performances and increase the material resistance without being exposed to light (dark), especially in the case of the MOVPE material. On the contrary, an H_2 annealing worsens the PD performances of both MOVPE and MBE deposited layers and generally results in more conductive material in the dark. The recorded changes upon thermal treatments, corroborated by theoretical calculations, suggest that the dissociation energies associated to H-related defect complexes are significantly lower in the case of κ-Ga_2O_3 with respect to β, allowing for such defects engineering (*i.e.*, redistribution) at temperatures well below the thermal stability window of the orthorhombic metastable polymorph. This work represents an important step further for the understanding of this material system and for its present and future application in different (opto) electronic devices and provides a viable comparison among κ-Ga_2O_3 layers deposited with two technologically relevant deposition techniques (MBE and MOVPE).

1. Methods

The orthorhombic κ-Ga_2O_3 thin films investigated in this work were deposited by MOVPE and MBE on c-plane sapphire substrates. MOVPE layers were synthesized from trimethylgallium (TMG) and ultrapure water precursors (H_2O/TMG flow ratio ≈ 200) with He as carrier gas (total pressure 100 mbar) at a growth temperature T_g = 650 °C. O-plasma assisted MBE with In-mediated metal exchange catalysis (MEXCAT) [39,40] allowed to grow κ-Ga_2O_3 on top of a 20 nm thick β-Ga_2O_3 nucleation layer [beam equivalent pressure $BEP_{Ga} = 3.4\times 10^{-7}$ mbar, $BEP_{In} = 1.3 \times 10^{-7}$ mbar, O_2-flux = 1 standard cubic centimeter per minute (sccm), plasma power P = 180 W, growth temperature T_g = 640 °C]. The thickness of all the investigated layers was between 500 and 700 nm. The MOVPE and MBE layers were cut in different pieces (about 5 × 5 mm^2) and some of them were ex-situ annealed (T = 500 °C, t_{dwell} = 2 h) in O_2 (naturally abundant ^{16}O as well as 97 % isotopic ^{18}O enriched) or H_2 in a tubular oven or in the MOVPE reactor chamber (1000 and 800 mbar, respectively). The κ-Ga_2O_3 layers (deposited as well as annealed) were structurally characterized by means of X-Ray diffraction (XRD) using both a Rigaku Smartly XE diffractometer and a PANalytical X'Pert Pro MRD with Cu Kα wavelength.

Resistive metal-semiconductor-metal (MSM) photodetectors were realized through the sputter-deposition of ohmic SnO_{2-x}/ITO/Au contacts through a shadow mask [41]. The characterized PDs had a 0.2 mm spacing between the linear contacts (length 4 mm) and the applied bias was 200 V (Keithley source-meter 2400, sensitivity 0.1 nA). Further details on the structure of the contacts as well as on the spectral response acquisition are reported in Ref. [32].

The XPS measurements were performed with a Scienta Omicron XPS-Lab (base pressure of 3 × 10^{-10} mbar) using a monochromated Al K_α source (hν = 1486.6 eV) at an angle of 54.7° with the Argus CU hemispherical analyzer. The energy resolution of the setup with a pass energy of 10 eV is 543 meV determined as the full width at half maximum FWHM of the Ag $3d_{5/2}$ peak. The core level measurements were performed at a pass energy of 20 eV with the source at 225 W (15 kV, 15 mA). A flood gun was used in order to compensate charging effects due to the semi-insulating nature of the samples. The core levels were aligned using the adventitious C 1s peak at 284.8 eV while for the valence band maximum (VBM) 50 % of the intensity were aligned at 0 eV.

The layers were also analyzed by means of ToF-SIMS (ToF-SIMS IV, IONTOF GmbH) depth profiling in negative polarity. The machine is equipped with an extended dynamic range detector, a high energy (25 keV) Ga^+ primary ion gun (raster size: 100 μm × 100 μm) and a low energy (1 keV) Cs^+ ion gun used for sputter-etching of the thin-films (raster size: 400 μm × 400 μm). Charge compensation was achieved by an electron flood gun. The crater depth was determined by interference microscopy and confirmed by profilometry.

Photoluminescence excitation PLE measurements were conducted using a Xenon arc lamp (XBO, PTI A500 with Osram 450W/4) which was monochromatized by a two-stage monochromator (2x Acton SpectraPro-275, 2400 l/mm gratings) resulting in a spectral bandwidth of the excitation of 1 nm [2]. The samples were mounted in a He-flow micro-cryostat (Janis ST-500) allowing for temperature dependent measurements between 5 K and 300 K. The optical excitation and detection of the emitted light was performed in back-reflection geometry using a UV fused silica beamsplitter and focusing lens (NA = 0.69). The emitted light was spectrally dispersed in a single-stage monochromator (Acton SpectraPro-300i, 120 l/mm grating) and detected by a thermoelectric-cooled charge-coupled device (Horiba Sincerity 2048x70-UVS). The PLE spectra were corrected by monitoring the excitation light in situ using a UV-optimized, high-sensitivity Si photodiode (Hamamatsu S4349) to account for the lamp's spectral power density and transmission losses across the optical setup and spectrally calibrated using neon and mercury gas discharge lamps.

Calculations to assess the bulk and defect-induced properties of κ-Ga_2O_3 were performed using the Heyd-Scuseria-Ernzhof screened hybrid functional (HSE06) [42] and projector-augmented wave (PAW) approach [43] as implemented in the VASP code [44,45]. The Ga 3*d* electrons were considered as explicit valence states and the Hartree-Fock mixing parameter was set to 32 %, and all unit cell calculations adopted a 500 eV plane wave cutoff and 6 × 4 × 4 Monkhorst-Pack k-point sampling. The optimized lattice constants for the orthorhombic unit cell were determined to be a = 5.03 Å, b = 8.64 Å, and c = 9.27 Å, which were used to construct a 120-atom supercell (a 3 × 1 × 1 repetition) for all defect calculations. All defect calculations adopted an energy cutoff of 400 eV, a 2 × 2 × 2 Monkhorst-Pack k-point sampling, and included spin polarization. Finite-size corrections for the formation energies of charged defects within the supercell approach were evaluated with the FNV method [46,47], using a calculated (The Materials Project [48]) low-frequency dielectric tensor with diagonal components $\varepsilon_{xx} = 15.79$, $\varepsilon_{yy} = 15.5$, and $\varepsilon_{zz} = 17.18$. Vertical transition energies for configuration coordinate diagrams were computed with energy corrections using the approach of Gake et al. [49] utilizing the calculated high-frequency dielectric tensor diagonal values of ε_{xx} =

4.30, $\varepsilon_{yy} = 4.23$, and $\varepsilon_{zz} = 4.20$. 1-dimensional configuration coordinate diagrams were used to evaluate the absorption and emission characteristics of relevant transitions at 300 K as described in Ref. [50].

1.1. Experimental results

The XRD analysis of the κ-Ga_2O_3 thin films highlights similar crystal quality for the MOVPE and MBE layers [Fig. 1 (a) and (b)]. Both are characterized by a three-fold rotational domain structure [φ-scan of the (122) κ-Ga_2O_3 reflections reported in Supplementary Information SI Figure S1] as already shown in Refs. [26,51]. The Rocking curve values for the (004) reflection [Fig. 1(b)] were about the same for the MBE and MOVPE samples (≈ 0.48°) qualitatively suggesting a similar mean rotational domain size distribution as discussed in Ref. [26]. The additional diffraction peak present for the MBE layer is related to a 20 nm thick (−201) epitaxial β-Ga_2O_3 nucleation layer [2θ ≈ 38.3° for the (−402) reflection, labeled as "nl" in the black curve of Fig. 1(a)] which is usually necessary in the In-mediated MEXCAT-MBE growth of κ-Ga_2O_3 on c-plane sapphire [40,52]. The left-side shift in the 2θ value of the (004) peak of the κ-Ga_2O_3 MBE layer with respect to the MOVPE one is related to a partial incorporation of In during the MEXCAT growth [39, 40,53]. The In cationic content has been quantified by calibrated SIMS (procedure discussed in Ref. [54]) to be about $3 \times 10^{20}\ cm^{-3}$, *i.e.*, around 0.8 cation % (SI Figure S2). Such In incorporation is not considered to play an important role in the current study, since *(i)* it is isovalent with Ga, *(ii)* it can generally be incorporated up to large percentages in the κ-$(In_xGa_{1-x})_2O_3$ alloy system without compromising the crystal quality or resulting in phase separation, and *(iii)* it does not affect significantly the bandgap of the material (*i.e.*, the overall PD characteristics) if the degree of In incorporation is below 1 cation % (as the one of the MEXCAT-MBE layer here investigated) [53].

These layers were cut in different equivalent pieces and some of them were *ex-situ* thermal treated (T = 500 °C, t_{dwell} = 2 h) in different atmospheres. The annealing temperature here employed is well below the κ to β phase transition one (T ≥ 700 °C) [55] and the XRD scan before and after annealing did not show any detectable difference (SI Figure S1).

PDs were fabricated with the as deposited and annealed MOVPE and MBE layers. The respective dark currents, as well as the responsivity curves (*i.e.*, electrical response at different wavelengths normalized by incident power – see Ref. [32] for further details) are reported in Fig. 2(a and b). The measured current without provided illumination (*i.e.*, dark current I_{Dark} at 200 V bias) for the MOVPE layers [Fig. 2(a)] is affected by the thermal treatments. In particular, while an O_2-annealing is found to reduce it of a factor three ($I_{Dark-MOVPE,as\ deposited} \approx 3\ nA$, $I_{Dark-MOVPE,O2} \approx 1\ nA$), a H_2-annealing is found to exhibit the opposite behavior increasing I_{Dark} by about one-and-a-half orders of magnitude ($I_{Dark-MOVPE,H2} \approx 100\ nA$). The responsivity curves highlight that the O_2-annealing significantly improves the solar blind characteristic of the MOVPE-based PD with respect to the one fabricated with the as-deposited sample [λ ≈ 300–650 nm range highlighted in yellow in Fig. 2(a)], with little reduction in the bandgap response. The rejection ratio, defined as $R_R = responsivity_{\lambda=250\ nm}/responsivity_{\lambda=500\ nm}$, improved for the MOVPE layer by one order of magnitude upon O_2-annealing with respect to the as deposited sample ($R_{R-MOVPE,O2} = 1.4 \times 10^5$ and $R_{R-MOVPE,as-dep} = 1.3 \times 10^4$). On the other hand, in the case of the H_2 treatment, the overall responsivity curve is shifted to higher values and the resulting PD characteristics significantly worsens with respect to the as-deposited MOVPE layer ($R_{R-MOVPE,H2} = 1.7 \times 10^3$).

In the case of the MBE-based PDs, both the dark current and responsivity curves were unaffected by the O_2-annealing with respect to the PD fabricated with the as-deposited layer ($I_{Dark-MBE,as\ deposited} \approx I_{Dark-MBE,O2} \approx 0.3\ nA$, $R_{R-MBE,as-dep} = 2.6 \times 10^4$ and $R_{R-MBE,O2} = 2.4 \times 10^4$). On the other hand, similarly to the MOVPE samples, the H_2-annealing increased the dark current and up-shifted the responsivity curve of the MBE layer, with a little improvement in this case of its rejection ratio ($R_{R-MBE,H2} = 4.1 \times 10^4$).

A direct comparison among all the investigated PDs allows to highlight the overall lower I_{Dark} recorded for the MBE samples (both as deposited and annealed) than those of the corresponding MOVPE samples. Nonetheless, the PD fabricated with the O_2-annealed MOVPE layer shows the best R_R among the analyzed samples.

On-off cycles ($\lambda_{On} = 250\ nm$, $t_{on-off} = 110\ s$, τ_{ON-OFF} calculated as time to go from 10 % to 90 % of photocurrent and vice-versa, see Fig. 3) qualitatively show for both MOVPE and MBE based PDs the overall fastest response upon O_2- ($\tau_{ON_OFF,MOVPE\ as-dep} = 39.6\ s\ _\ 26.4\ s$, $\tau_{ON_OFF,MBE\ as-dep} = 35.9\ s\ _\ 9.5\ s$; $\tau_{ON_OFF,MOVPE\ O2} = 29.6\ s\ _\ 3.1\ s$, $\tau_{ON_OFF,MBE\ O2} = 37.6\ s\ _\ 5.0\ s$) and the slowest upon H_2-annealing ($\tau_{ON_OFF,MOVPE\ H2} = 37.0\ s\ _\ 66.4\ s$, $\tau_{ON_OFF,MBE\ H2} = 39.5\ s\ _\ 40.9\ s$).

Combining the responsivity curves (Fig. 2) and the time response (Fig. 3) of the analyzed PDs it is possible to highlight that *(i)* the as deposited MBE material seems to be better performing as PD with

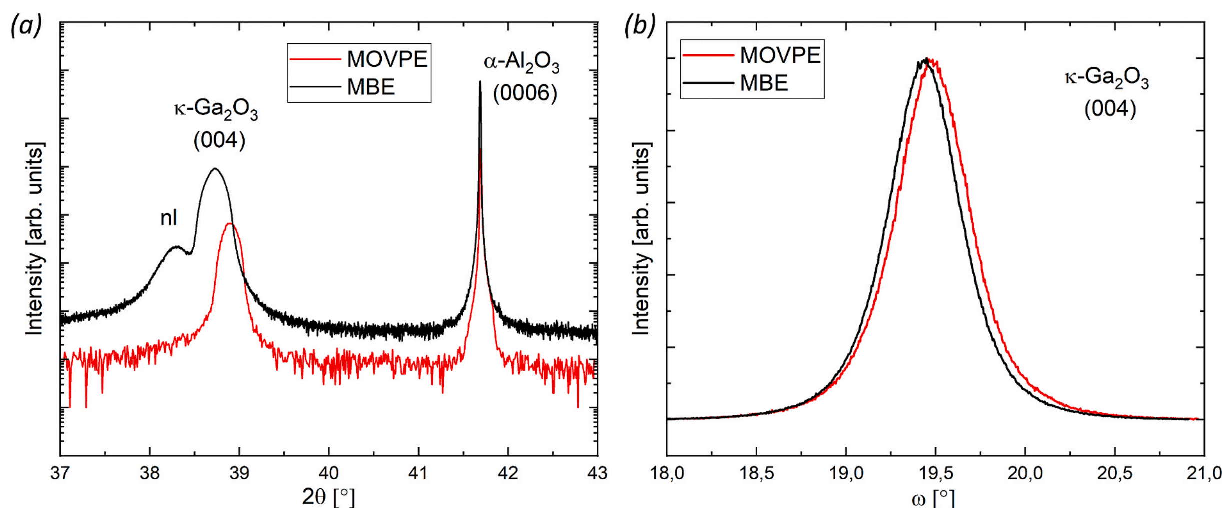

Fig. 1. Symmetric out-of-plane (a) 2θ-ω (not normalized, logarithmic scale) and (b) ω (normalized, linear scale) XRD scans of the as deposited MOVPE and MBE κ-Ga_2O_3 as-deposited layers (red and black curves, respectively) on c-plane sapphire. In (a) for the MBE layer, "nl" stands for a 20 nm thick epitaxial β-Ga_2O_3 nucleation layer [(-402) reflection]. Measurements performed with monochromatic Cu $K\alpha_1$ radiation. (For interpretation of the references to colour in this figure legend, the reader is referred to the Web version of this article.)

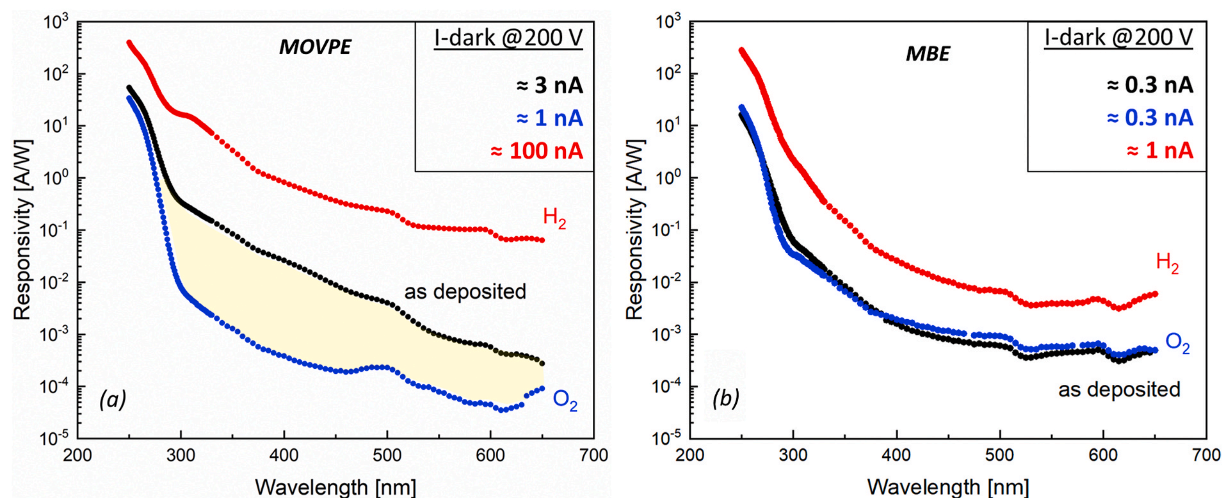

Fig. 2. Photodetector responsivity (*i.e.*, electrical response at different wavelengths normalized by incident power) of (a) MOVPE and (b) MBE deposited κ-Ga_2O_3 layers as-deposited, O_2- and H_2-annealed (black, blue, and red curves, respectively). The respective dark currents measured at 200 V bias are reported in the insets. The yellow region in (a) highlights the significant drop of responsivity in the 300–600 nm range for the O_2-annealed material with respect to the PD fabricated with the MOVPE as-deposited material. (For interpretation of the references to colour in this figure legend, the reader is referred to the Web version of this article.)

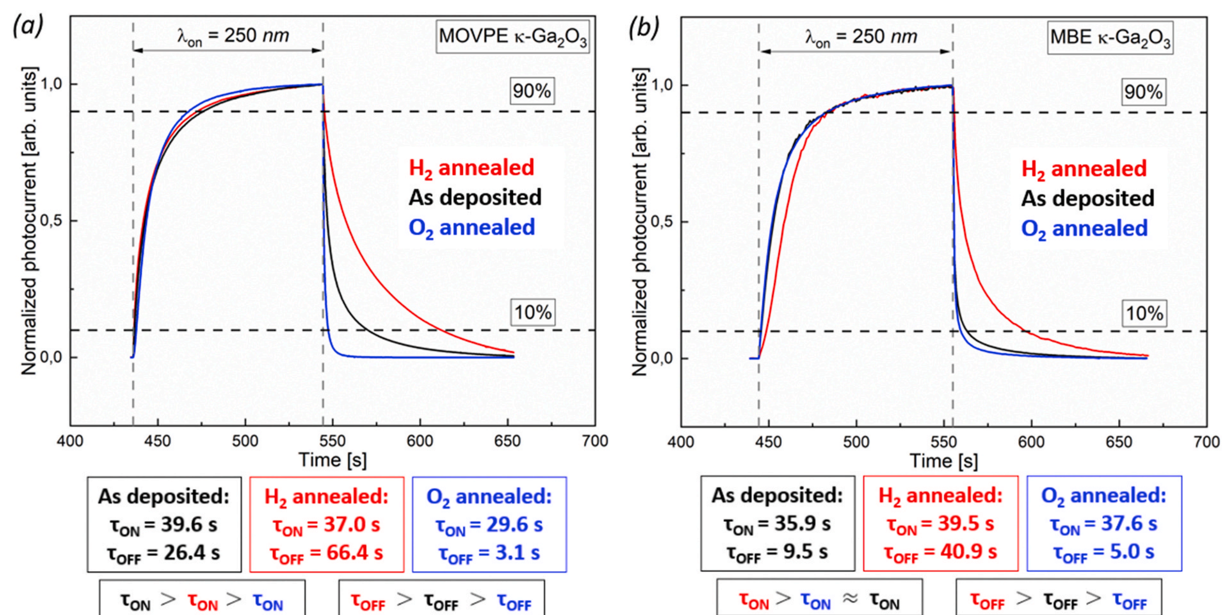

Fig. 3. Normalized current for PDs fabricated with (a) MOVPE and (b) MBE layers. The current has been reported for the 3rd acquired cycle; all the acquired non-normalized cycles are reported in the SI (Fig. S3).

respect to the MOVPE as deposited one and *(ii)* the overall beneficial role of the O_2 annealing on the time response of the κ-Ga_2O_3 based PDs, with the MOVPE O_2-annealed one resulting in the best performing photodetector. In this framework, it should be specified that this work does not focus on the overall optimization of the PD performances, but rather on the understanding of the point defects in the κ-Ga_2O_3 material system; in fact, we highlight that the control of *e.g.*, PD device architecture, applied bias, illumination conditions, can have significant effects on *e.g.*, the dark current, rejection ratio, photo-gain, and response time [56,57].

A similar beneficial effect on PD performance (responsivity and on-off cycles) upon O_2 or air annealing of MOVPE κ-Ga_2O_3 layers was reported in a recent work by Li et al. [58], that suggested the V_O-filling to be responsible for such recorded behavior - mostly based on XPS investigation. We have also performed an XPS investigation on all the studied MOVPE and MBE samples. The O1s core level peaks of the MOVPE samples are shown in the SI Figure S4 and can be treated as the convolution of two separate contributions, *i.e.*, an O_I component related to the lattice oxygen and an O_{II} one probably related either to adventitious hydroxyls of water [59] or to carbonate contaminations [60,61]. In fact, it is common to observe signatures in the O1s XPS spectra around 532.5–533/531.2–531.8 eV due to hydroxyl (-OH) groups [59] / carbonates [60] that can be commonly present on the surface of the sample, with their concentration being possibly affected by thermal treatments/atmospheres. Experimental evidence of the (-OH) groups and their effects on the O 1s peak has been already observed for the β polymorph of Ga_2O_3 [62]. In their work Li et al. [58] observe a decrease in the O_{II}/O_I ratio after the annealing treatment in O_2, suggesting a possible partial V_O filling in the thermal treated layer probed depth as an explanation. As shown in SI Figure S4 Fig. S4 we also observe a similar result for the MOVPE layers, as well as an increase in the O_{II}/O_I after H_2-annealing. Even if we cannot exclude the possibility of affecting the

overall concentration of V_O upon the tested annealing conditions in the probed volume, we believe that the reduction of the O_{II} component after O_2-annealing, as well as the increase after H_2-annealing, is given by a variation in the (-OH) group at the surface. In fact, an annealing in O_2 could potentially reduce the amount of (-OH) groups due to desorption, while an annealing in H_2 could instead increase this amount. As for the O1s core level peaks of the MBE layers (SI Figure S5), even though it is found to be affected by the thermal treatments in different atmospheres, a direct comparison with the MOVPE layers could be misleading. In fact, the employment of the MEXCAT growth in MBE results in a surface segregation/accumulation of the catalyst element [63] (in the current case In, see XPS survey spectra reported in SI Figure S5) that could itself affect the shape of the O1s levels and their relative change upon thermal treatments. Additional analysis on the Ga 2p and 3s core levels for all the investigated samples are reported and commented in the supplementary information (SI Figure S6).

A comparison for the VBM is provided in Fig. 4. Interestingly, the MOVPE as-deposited sample is the only one that shows a small shoulder peak inside the bandgap [in-gap states highlighted by arrow in Fig. 4 (a)]. This is most likely related to deep energy level defect states as already observed in similar MOVPE κ-Ga_2O_3 samples [64]. Using the linear extrapolation method to estimate the VBM will put this in-gap states around ~ 2.2 eV above the VBM. However, Swallow et al. [62]. demonstrated how this method tends to underestimate the VBM by ~ 0.5 eV for β-Ga_2O_3. Due to the similarities in the VB structure of the κ and β polymorphs [52] if we then apply this correction to our VBM estimation this will locate the in-gap states at ~ 2.7 eV above the VBM instead. After the annealing process, independently from the annealing environment (H_2 or O_2), the in-gap states cannot be detected anymore. It is important to highlight that not even the as deposited MBE layer shows in-gap states, pointing towards an initial different distribution of deep level defects associated to the two investigated deposition techniques.

We stress that the experimental findings on the PDs performances indicate a change in the point defects distribution across the entire film thickness, while XPS is a surface sensitive technique that can provide information just limited to the very-first nanometers of the investigated layers (SI Table S1).

Moreover, to get experimental data on the possible incorporation of oxygen upon mild O_2-annealing treatments, an as-deposited MOVPE layer was exposed to an oxygen background pressure of stable ^{18}O isotopes in an identical thermal cycle to the ones previously investigated; this has been followed by a depth-resolved ToF-SIMS measurement and compared to the depth profile acquired on an as-deposited layer. The resulting isotope fraction (SI Figure S7) shows a partial penetration (limited to the first 5–10 nm from the surface of the layer) of the ^{18}O isotopes. From the ^{18}O penetration profile, we estimate a diffusion coefficient of the order of 10^{-17} cm^2s^{-1}. The observation of a penetration profile tells us that oxygen ions diffuse in this material at this temperature, but it does not reveal by what mechanism (vacancy, interstitial or interstitialcy) nor along which path (through the lattice or along extended defects [26]) the ions diffuse. A deeper analysis would require, in addition to solid evidence of mechanism and of path, quantitative information concerning the concentration of the point defects.

Additionally, all the MBE and MOVPE as deposited and annealed layers characterized as PDs were analyzed with depth-resolved ToF-SIMS. The level of Si impurities (possibly playing the role of shallow donors [26,65]) was on the edge of the detection limit of the ToF-SIMS ($\approx 2 \times 10^{17}$ cm^{-3}, SI Figure S8). It is also worth mentioning that a quantitative analysis of hydrogen in the as-prepared and annealed samples by means of ToF-SIMS was not possible, because of residual gas adsorption onto the sample in the UHV chamber during analysis. In fact, analysis of H-implanted β-Ga_2O_3 single crystals (peak concentration of 7 $\times$ 10^{19} cm^{-3}) under optimized UHV conditions revealed no implantation profile, thus setting here the lower limit of H detection in our system to 7×10^{19} cm^{-3}. Unsurprisingly, the carbon intensity profiles obtained for the analyzed layers were also affected by residual gas adsorption and thus no reliable data for C levels in the films were obtained.

The set of MOVPE and MBE samples was also investigated with PLE and PL spectroscopy. The PLE spectra displayed for integrated detection energies of the entire luminescence bands (between about 1.8 and 4.0 eV, see PL in Fig. 6) for all the investigated MOVPE and MBE layers are displayed in Fig. 5 and in the SI Figure S9(T = 300 K as well as T-series down to 5K, respectively). While MBE deposited layers are similar in the absorption onset, *i.e.*, largely independent of the post growth annealing treatment, the MOVPE ones show below the band edge (4.5–4.9 eV) clear shifts with lowest energy for H_2- and highest for O_2-annealing [Fig. 5(a)]. A direct comparison between MBE and MOVPE layers [Fig. 5 (b)] highlights that the two spectra show the strongest difference for H_2-annealing, while very similar excitation to the MBE ones is recorded when the MOVPE layer is annealed in O_2. We note that PLE spectroscopy suggests the energy gap of κ-Ga_2O_3 to be about 5 eV, *i.e.*, slightly higher with respect to the one of the β polymorph. This is in good agreement with previously reported theoretical calculations [66].

The temperature dependence of the PLE spectra (SI Figure S9) is invariant for the MBE layers down to 5 K, consistently with the observation at 300K [Fig. 5(a)]. The as-deposited and O_2 annealed MOVPE samples share a similar T-dependence; differently, the H_2-annealed MOVPE one shows pronounced excitation of PL via sub-bandgap states

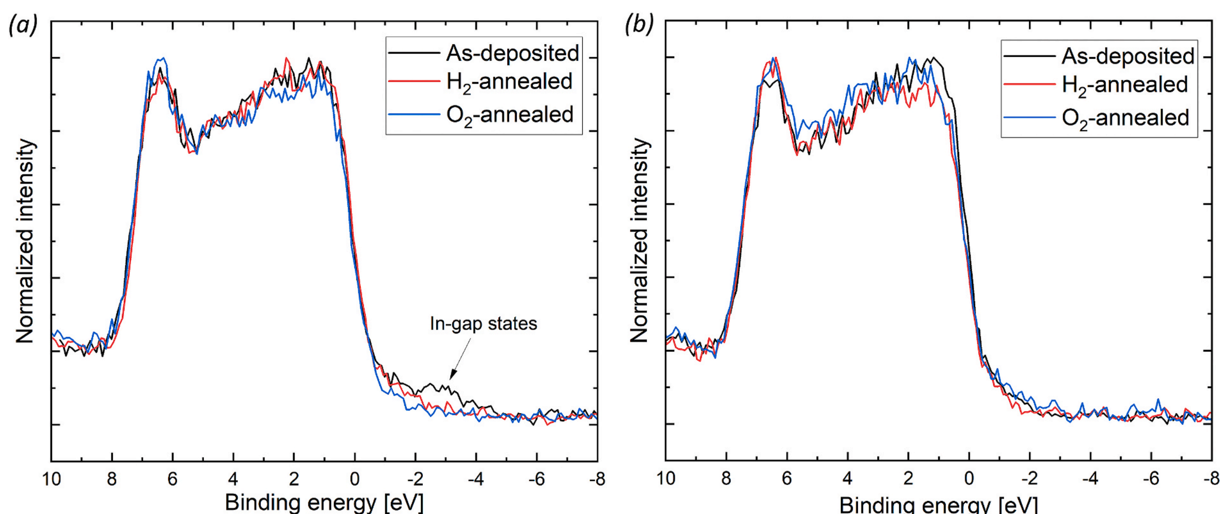

Fig. 4. XPS Valence band spectra of the (a) MOVPE and (b) MBE samples. The 50 % intensity of the VBMs were aligned at 0 eV for direct comparison.

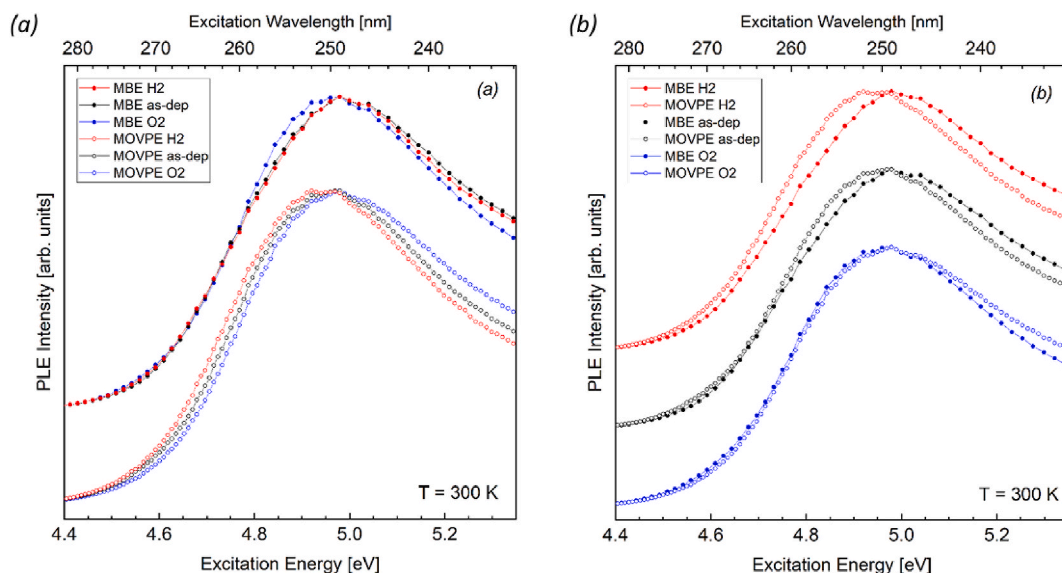

Fig. 5. Normalized photoluminescence excitation (PLE) spectra of as grown, O_2, and H_2 annealed (black, blue, red respectively) MOVPE and MBE (empty and filled circles) κ-Ga_2O_3 thin films measured at T = 300 K. The two graphs are reporting the same data, but are displayed with the aim to directly compare (a) the layers with the same deposition technique (MOVPE or MBE) but diferent thermal treatments (as deposited, O_2, H_2) and (b) the same thermal treatment but different deposition technique. PLE spectra are displayed for integrated detection energies of the entire luminescence bands between about 1.8 eV and 4.0 eV. (For interpretation of the references to colour in this figure legend, the reader is referred to the Web version of this article.)

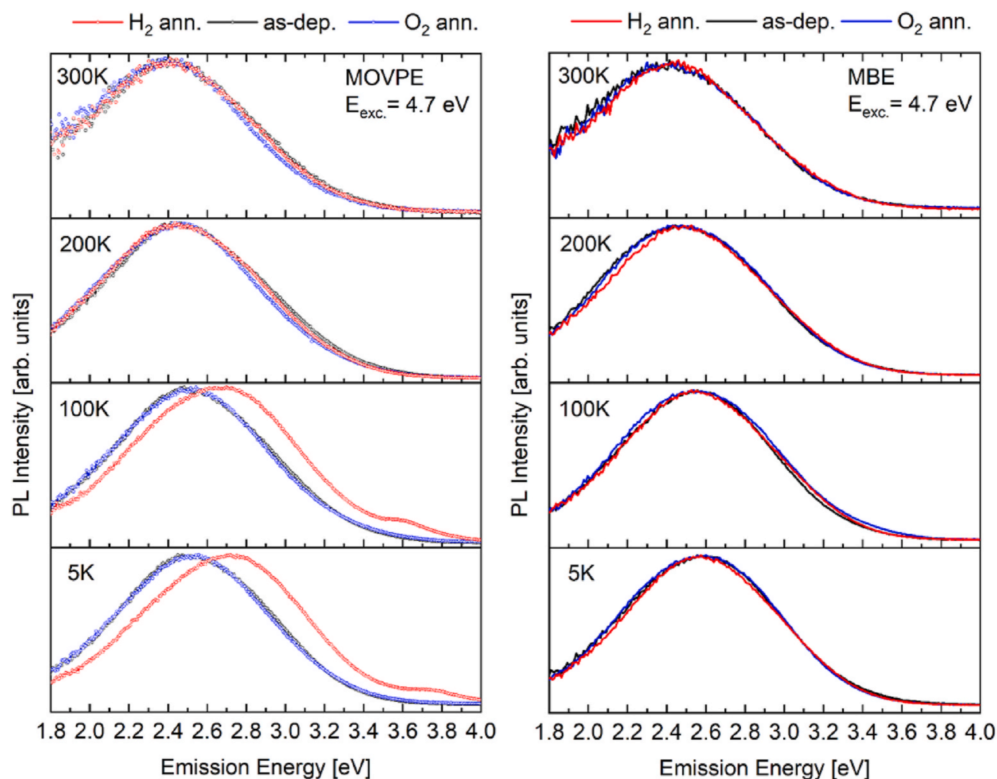

Fig. 6. PL spectra of as-deposited, O_2, and H_2 annealed MOVPE and MBE κ-Ga_2O_3 thin films measured at temperatures of T = 5K, 100K, 200K, and 300K. Spectra are shown for sub band edge excitation at 4.7 eV.

between 4.4 and 4.9 eV at temperatures lower than 100 K.

The PL spectra were analyzed for different excitation energies. Fig. 6 and SI Figure S10 show the collected PL for excitation energies below (4.7 eV) and above (5.2 eV) the bandgap, respectively. Generally, a convoluted broad band between about 1.8 and 3.5 eV can be observed, qualitatively in line with previous cathodoluminescence measurements on κ-Ga_2O_3 epitaxial layers [67]. For above bandgap excitation (SI Figure S10) an emission maximum is found at about 2.4 eV at room-T, while the T-reduction leads to a spectral shift to higher energies (about 2.7 eV) for all samples; no significant variation among them can be highlighted (despite annealing or different deposition technique).

For sub-band edge excitation (Fig. 6) the room-T PL spectra of MBE

and MOVPE samples are once more mostly independent of post-growth annealing (similar to above band edge PL). Also in this case the emission maximum at room-T is at around 2.4 eV, but its T-dependent shift is less pronounced than for the 5.2 eV excitation for all the analyzed layers (emission maximum at about 2.6 eV) with the only exception of the MOVPE layer annealed in H_2: in this case a pronounced difference is recorded for temperatures ≤100 K. The PL of the MOVPE H_2-annealed sample is significantly shifted to higher energies as compared to the other two MOVPE layers (maximum around 2.8 eV). In addition, a weak luminescence band around 3.6 eV–3.8 eV becomes visible in this sample that shifts to lower energies and decreases in intensity with increasing temperature (from 5 K to 100 K). To further investigate this weak luminescence band, the T-dependent excitation spectra for a detection energy of 3.6 eV–3.8 eV is reported for the MOVPE layers in the SI Figure S11. At temperatures of 100 K and 5 K a new excitation channel below the bandgap becomes visible exclusively in the H_2 annealed MOVPE sample. In contrast, the as deposited and O_2 annealed MOVPE layers exhibit excitation spectra that are similar to the MBE ones (not shown) and those with integrated detection energies between 1.8 and 4.0 eV (SI Figure S9). At 5 K, the excitation channel of the MOVPE layer annealed in H_2 is centered around 4.7 eV, *i.e.*, 300 meV below the bandgap energy of about 5.0 eV at 5 K. Therefore, a rather shallow state at 4.7 eV (300 meV below CB, visible in PLE of SI Figure S11) gives rise to a 3.7 eV luminescence transition (recorded in the PL spectra of Fig. 6).

The collected experimental data suggest that the overall changes induced by mild annealing treatments on the κ-Ga_2O_3 layers *(i)* must be related to both shallow as well as deep level defects, *(ii)* involve most of the layer thickness, and *(iii)* the recorded effects upon different background atmospheres are not of the same magnitude for MOVPE or MBE deposited material (although the trends are qualitatively similar).

1.2. Theoretical calculations

Similar to the low-symmetry β-phase, κ-Ga_2O_3 exhibits a number of symmetrically distinct O and Ga sites that can differ in formation energy and contribute to different defect levels within the band gap. We performed a comprehensive set of theoretical calculations to evaluate the energetics of the six distinct O sites (O1–O6), and four distinct Ga sites in κ-Ga_2O_3 (Ga1-Ga4), as well as their interactions with hydrogen. We adopt similar notation for sites as in references, [66,68] with Ga1 being tetrahedrally-coordinated, Ga2, Ga3 and Ga4 being octahedrally coordinated, with Ga3 and Ga4 exhibiting larger octahedral distortions with a single longer bond (also referred to pentahedral coordinations in literature [69]), and the O sites exhibiting 3-fold and 4-fold coordination. We include the formation energies of the native vacancies in Fig. 7 and summarize the transition levels calculated for the studied defects in SI Table S2. Similar to β-Ga_2O_3, we find for κ-Ga_2O_3 all isolated V_O to

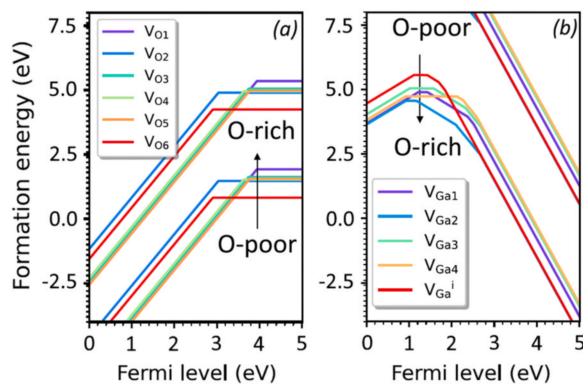

Fig. 7. Formation energy diagram for (a) oxygen vacancies and (b) gallium vacancies in κ-Ga_2O_3 shown as a function of the Fermi level for the limiting extremes of O-rich and O-poor (Ga-rich) conditions.

behave as deep double donors that are favorable under O-poor conditions, neutrally charged for sufficiently high Fermi energy E_F level positions (≥ 3 eV) typical of a *n*-type material [Fig. 7(a)] [70]. The V_{Ga} behave as deep acceptors with favorable formation under O-rich conditions for E_F level positions above 3 eV [Fig. 7(b)] that are again typical of a *n*-type material. Again similar to β-Ga_2O_3, we find that split Ga vacancies [71–75], [71–75] [71–75] V_{Ga}^i (*i.e.*, V_{Ga}- Ga_i -V_{Ga}) are also stable in the κ-phase, with the most favorable configuration found to be a site in between V_{Ga1} and V_{Ga4} sites, forming another distorted octahedrally-coordinated Ga species (SI Figure S12). We find that these sites exhibit large local minima similar to the V_{Ga}^i configurations in the β- and α-phases, with V_{Ga}^i being more stable than V_{Ga1}^{-3} in *n*-type conditions by ~0.6 eV, with a barrier of only 0.6 eV to form (more stable than V_{Ga4} by ~1.5 eV) [76]. Considering the similarities with the β-phase, the strong favorability of V_{Ga} and possibility of diffusion at modest temperatures indicates that V_{Ga} are likely mobile under the annealing conditions investigated in this work [77].

To evaluate the role of hydrogen in view of possible differences owing to the investigated deposition techniques and annealing treatments, we summarize the formation energies of several hydrogen-related defects in Fig. 8. The presence of hydrogen interstitials H_i in κ-Ga_2O_3 or when acting as a substitutional defect on an oxygen site (H_O) are found to behave nearly exclusively as shallow donors (*e.g.*, H_{O3}), with H_i being the most energetically favorable one especially in O-rich conditions [Fig. 8(a)]. This again is in line with previous calculations reported for β-Ga_2O_3 [70] and in accordance with experimental evidence on MOVPE deposited κ-Ga_2O_3 using H_2 as a carrier gas [26]. The only exception we find is for H_{O6}, which binds to a Ga4 and acts as a deep acceptor for Fermi levels above the (+/−) transition [4.58 eV above the VBM, see Fig. 8(a)]. The deep state associated with H_{O6} is analogous to β-Ga_2O_3, where the dimerization of tetrahedrally-coordinated, such as the Ga1 adjacent to the O6 site, lead to the lowest-lying states in the band gap as compared to the other coordination environments [78]. Interestingly, this suggests hydrogenation of oxygen-deficient material could lead to a combination of both shallow donor states from H occupying O1–O5 sites, as well as H_O that preferentially incorporate as compensating acceptors on the O6 site [the most favorable V_O site in *n*-type conditions from Fig. 7(a)].

When considering the stability of the H_O, we evaluate their defect binding energies, which we define as the formation energy of the complex relative to the isolated constituents (*e.g.*, H_i^+ and each type of V_O). We summarize the results in Fig. 9, where we find that H_O is only stable in *n*-type conditions, with modest binding energies ranging from ~0.5–1.3 eV depending on the O site occupied. Considering the modest binding energies and the low migration energies for H_i in other Ga_2O_3 polymorphs [76,79], this suggests that H_O are likely to dissociate at even lower temperatures than those of the annealing ones here investigated; this can free more mobile H_i that can out-diffuse from the sample or interact with other defects in the lattice. Indeed, persistent changes in the electrical conductivity of extrinsically doped κ-Ga_2O_3 layers upon thermal treatments below 500 °C were already highlighted in previous articles [30,80].

Beyond shallow donor configurations, a large amount of literature on the β-Ga_2O_3 polymorph suggests that its defect chemistry is majorly affected by complexes involving V_{Ga}, with hydrogenated V_{Ga}-H appearing to play a fundamental role as deep acceptors [36,72,73,76,78,81]. In Figs. 8 and 9 we also include the formation energy and stability of various V_{Ga}-H-related complexes for κ-Ga_2O_3. Fig. 8(b,c,d) shows how multiple H species can be favorably trapped at V_{Ga}, especially in (but not limited to) O-rich conditions. For hydrogenated V_{Ga}, the levels relevant for *n*-type samples move deeper into the band gap (closer to the valence band edge) depending on the coordination environment and hydrogenation state (SI Table S2). V_{Ga} can be readily hydrogenated with very low formation energies in *n*-type conditions (Fig. 8) and binding energies that can approach 2.5 eV in *n*-type conditions for the first hydrogen, and can still exceed 1 eV for a 3rd hydrogen that electrically

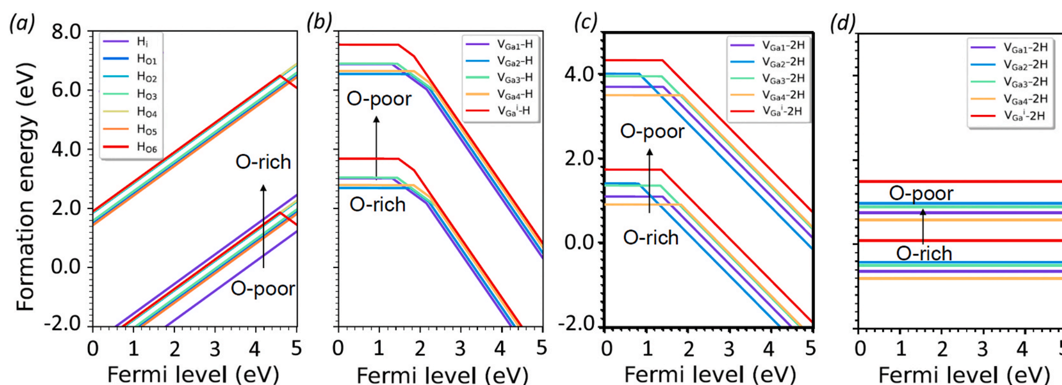

Fig. 8. Formation energy diagram for H interstitials (H_i) and their complexes with oxygen vacancies (a), and their complexes with gallium vacancies with 1H (b), 2H (c) and 3H (d), shown as a function of the Fermi level for the limiting extremes of O-poor and O-rich conditions.

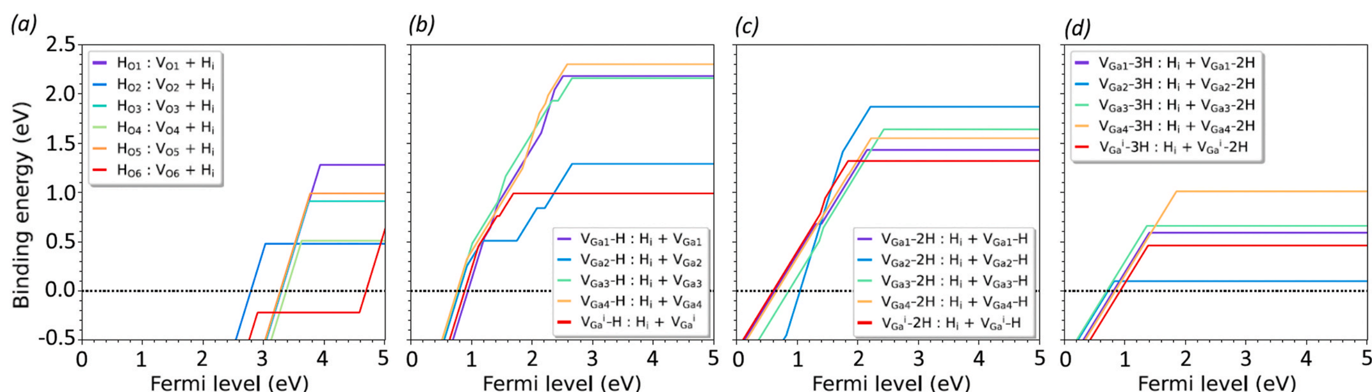

Fig. 9. Plot of the calculated binding energies for hydrogen-related complexes with respect to (a) singly-hydrogenated V_{Ga}-H, (b) doubly-hydrogenated V_{Ga}-2H, (c) triply-hydrogenated V_{Ga}-3H, and (d) in oxygen sites H_O. The binding energies are calculated as a function of the Fermi level according to the formation energies labeled in the legends, where a positive binding energy indicates a favorable complex with respect to the isolated constituents.

passivates the complex (Fig. 9). We note that as for the other neutral isolated and hydrogenated V_{Ga} configurations, the fully-passivated V_{Ga}-3H complexes in Fig. 8(d) can also exhibit a polaronic-like (+/0) transition level approximately 1 eV above the VBM. Interestingly we find the V^{i}_{Ga}, which is the most stable isolated V_{Ga} in *n*-type conditions, binds H weaker than the other on-site vacancies and the split vacancies in the β-phase. Therefore, qualitatively the picture is very similar to the one calculated for β [76], with the only exception related to the binding energies of such complexes that are significantly lower for κ-Ga_2O_3 (in β-Ga_2O_3 the most stable V_{Ga}-H complex configuration can approach the 3.4 eV[76]). In this regard, considering similar frequencies of the V_{Ga}-H vibrational modes calculated for β and a similar probability of dissociation [76], a large number of hydrogenated V_{Ga}-H complex configurations could be dissociated at temperatures in the range of 500 °C (with respect to the significantly higher 800 °C necessary to dissociate them in the β polymorph). This suggests that annealing temperatures and environments can likely influence the relative populations and passivation state of hydrogenated cation vacancies in κ-Ga_2O_3 more strongly than in

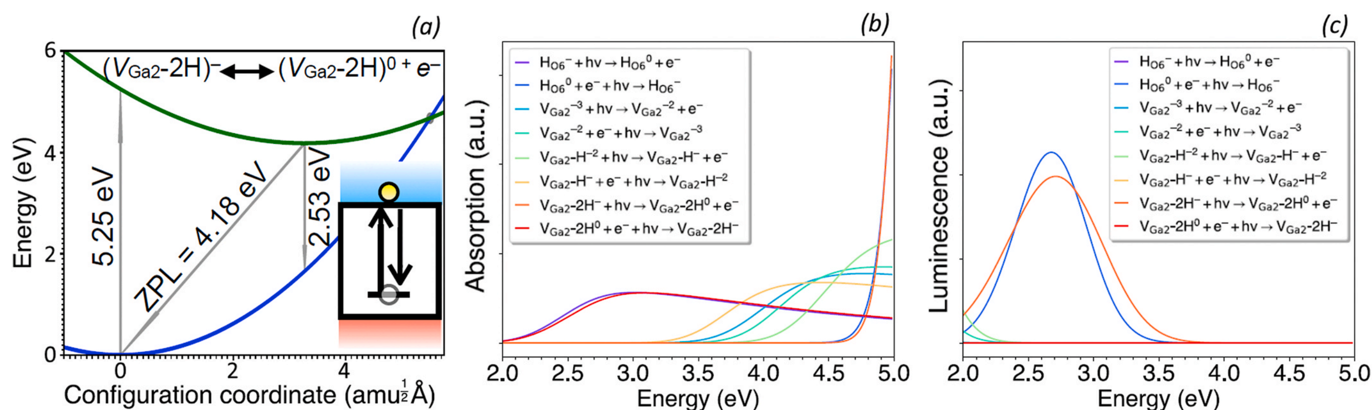

Fig. 10. (a) Example configuration coordinate diagram calculated for optical transitions associated with ionizing an electron on a $(V_{Ga2}\text{-}2H)^{-}$ complex to the conduction band, showing the calculated absorption, zero-phonon, and emission lines. (b) Absorption and (c) emission profiles calculated for the defects and transitions listed in the legend that would be most relevant in *n*-type conditions.

β-Ga_2O_3.

To provide additional characterization of some of the optical transitions associated with defects, we also performed a configuration coordinate diagram analysis of the optical excitations associated with transitions to and from the localized states associated with defects found to be favorable in Figs. 7 and 8. We include results in Fig. 10 for the H_{O6} and the non-hydrogenated and hydrogenated octahedral V_{Ga2} (absorption and emission profiles calculated following the approach detailed in Ref. [50]) as representative examples and discuss them in more detail in the following section.

2. Discussion

The combination of theory and experiments results in a rather comprehensive picture of the point defects redistribution in κ-Ga_2O_3 thin films deposited with MOVPE and MBE upon mild annealing treatments, with the effect being dependent on the background atmosphere. The recorded behavior of PDs (Figs. 2 and 3) as well as PLE and PL results (Figs. 5 and 6) are compatible with an overall change of shallow and deep level defects that should involve most of the layers thickness, with this picture being supported by DFT calculations. As for deep levels, our experimental data (^{18}O stable isotopes diffusion profile, SI Figure S7) cannot exclude a possible role of deep donor states associated with oxygen vacancies that would be annihilated under O-rich annealing environments. Nonetheless, the changes recorded in XPS spectra for the O1s core level upon annealing treatments in different atmospheres cannot be attributed to different oxygen stoichiometries of the layers [58] (SI Table S1, SI Figs. S4, S5, S6), but are most likely related to a variation in the surface adsorbates. Sufficiently mobile species at the temperatures and times adopted during the investigated annealing treatments must be involved in the point defects redistribution. In this framework, hybrid functional DFT calculations, supported by PL and PLE spectroscopy, highlight V_{Ga} and various H-related defects (Figs. 7, Figure 8, Fig. 9) to be likely involved in the recorded trends. The simplistic band diagram sketch reported in Fig. 11 aims at summing up the theoretically predicted energetic position of the most favorable defect levels (intrinsic as well as H-related) in κ-Ga_2O_3 and is helpful for the following discussion. It is worth to mention that, given the already complicated framework of this metastable polymorph, we have here decided not to consider in the following discussion the possible important role of vertically oriented structural defects (*e.g.*, rotational domains – see SI figure S1) in mediating the concentration/distribution as well as the in- and out-diffusion of point defects in all the κ-Ga_2O_3 layers here investigated.

We start from the as-deposited MBE and MOVPE layers. The significantly different $I_{Dark,as\ deposited}$ collected on the PDs realized from these two as-deposited layers points towards a lower concentration of shallow defects in the MBE grown material. We suggest this to be mostly related to a different initial level of hydrogen between the MBE and MOVPE deposited layers; in fact, we found that H located at interstitial- or most of the O-sites results in shallow donor states in κ-Ga_2O_3 (Fig. 8). Indeed, it is reasonable to assume a larger concentration of H in the MOVPE deposition environment with respect to the MBE one – *i.e.*, metalorganic (TMG) and the oxidizing (H_2O) precursors in MOVPE. Nonetheless, other extrinsic elements (*e.g.*, C) could also play an important role in determining the distribution of point defects in the as-deposited material according to the two different growth techniques. C substitutionals and C–H complexes have been already found to play an important role in the β-Ga_2O_3 material system as shallow donor as well as deep acceptor level defects [79]. Again in MOVPE it is conceivable that a higher level of C is present in the as-deposited layers (*e.g.*, by the use of metalorganic) with respect to the MBE grown ones. We were not able to reject, however, the possibility of different C-related defects levels between the MBE and the MOVPE layers. Generally, the presence of a higher concentration of defects in the as-deposited MOVPE layer with respect to the MBE one is also independently suggested by the faster response at band gap excitation of the latter (Fig. 3) and the deep level defects band visible just in the as deposited MOVPE layer by XPS investigation (Fig. 4).

The mild annealing treatments (T = 500 °C, t = 2h) in different background atmospheres (H_2, O_2) on the as deposited MBE and MOVPE layers are found to affect their functional properties. Generally, MOVPE layers show much larger changes (PD performances and luminescence spectroscopy) upon thermal treatments in both annealing environments with respect to the MBE ones. In particular, an O_2 annealing is found for MOVPE layers to significantly enhance the performances of the related PDs in terms of solar blindness, dark current, and a significantly faster transient at the gap light (Figs. 2 and 3). Given the modest binding energies calculated for H_O-related defects and for some of the hydrogenated V_{Ga}-complexes (Fig. 9), the possibility of complex dissociation and defect evolution under the studied conditions is more likely in the MOVPE samples and may explain this response. For the O_2 annealed MBE layer the effect on the responsivity curve and dark current is negligible with respect to the as deposited material (Fig. 2), and just a slight improvement in the τ_{OFF} is recorded (Fig. 3). H_2-annealing of the as deposited layers leads for both MOVPE and MBE material to an increased dark current and responsivity at the gap, but with significant worsening of the solar blind characteristic of the related PDs (Fig. 2) also in terms of transient times (Fig. 3). Also, for the H_2-annealing the effects are significantly larger in the MOVPE samples. The enhanced photo-gain and the longer response time at the gap (on-off cycles) evidenced in the H_2 annealed sample (Figs. 2 and 3) can be related to the presence of carrier traps [32]. In fact, trapping times longer with respect to the photocarrier transit time can result in an excess of the collected charge at electrodes when considering the number of photogenerated carriers per unit time in the irradiated volume (*i.e.*, photo-gain higher than unity); moreover, the decay time of the photocurrent is influenced on emission and capture rate of the traps. These points also support a higher defects density in the MOVPE samples. In the H_2-annealed layers deposited by MOVPE, photo-gain increases in the whole investigated spectral range overcoming the dark current, even if the latter is increased by an enhanced density of shallow H_2-donors. Note that due to the long response time of the traps, also a distortion of the responsivity curve of the latter samples can be expected, depending on the duty cycle of the acquisition routine. All of these facts agree with the hypothesis that hydrogen influences the carrier emission and capture properties of deep levels and the density of traps, likely through forming complexes with defects like V_{Ga} deep acceptors, which are thus controlled by the annealing atmosphere.

A comparison of the PLE and PL spectra further supports this picture, consistently highlighting detectable differences upon annealing treatments in the MOVPE layers, while the MBE layers do not show significant enough variations even considering the annealing treatments. The shift to lower energies in the absorption onset in the PLE spectra for the entire luminescence bands of the MOVPE layers (Fig. 6) suggests the possibility to significantly decrease or increase (O_2 and H_2 annealing,

Fig. 11. Simplified band-diagram sketch reporting some of the most energetically favorable defect levels in κ-Ga_2O_3 from theoretical calculations (Figs. 7 and 8 as well as SI Table S2). Energies are given relative to the valence band maximum.

respectively) the concentration of shallow donors (H_i and H_O in most configurations, Figs. 8, Figs. 9 and 11). As for deep level defects we focus our discussion on the PL spectra reported in Fig. 6. The highlighted convoluted broad band is peaked for all MOVPE and MBE samples at around 2.4–2.5 eV (300 K and 5 K, respectively) with the only exception of the H_2-annealed MOVPE layer that shows a significantly different T-dependance: for low temperatures *(i)* its maximum shifts to about 2.8 eV at 5 K and *(ii)* a weak luminescence band located at around 3.8 eV at 5 K related to an excitation channel centered at around 4.7 eV (SI Figure S9) appears. The calculated absorption and luminescence spectra for several of the most favorable candidate defects are summarized in Fig. 10(b and c). We find that both the H_{O6} and V_{Ga2}-2H exhibit luminescence spectra that favorably agree with the experimental PL spectra reported in Fig. 6 considering the emission arising from optically-excited V_{Ga2}-2H, such as from an electron in the conduction band recombining with the $(V_{Ga2}\text{-}2H)^0$ [Fig. 10(b and c)]. Regarding point *(i)* of the H_2-annealed MOVPE sample, some emissions arising from transitions associated with ionized H_{O6} are similar in energy to those associated to V_{Ga2}-2H and could possibly contribute to the multiple peaks and their stronger temperature dependence experimentally observed (Fig. 6). We note that non-hydrogenated forms of V_{Ga} have lower-energy transitions (both absorption and emission, Fig. 10) and are not as good of a match as more hydrogenated forms. Regarding *(ii)* the weak luminescence band in the H_2-annealed MOVPE layer could be related to a transition level at about 1 eV above the valence band maximum: this estimation is based on the observation of an excitation channel at about 4.7 eV (SI Figure S11), *i.e.*, 0.3 meV below the CB, that gives rise to an emission band with an energy of 3.7 eV (Fig. 6). We notice that an H_2-annealing is likely to result in further hydrogenation of V_{Ga}-related defects, generally resulting in their defects energy levels moving closer to the VBM (Fig. 11). Moreover, given the propensity for rapid hole localization in Ga_2O_3 polymorphs [66,82], [66,82–84] [66,82–84] passivated forms of V_{Ga}-related complexes are expected to rapidly trap holes, leading to polaronic states in the vicinity of 1 eV above the VBM with values differing within ~0.1–0.2 eV based on details of the atomic relaxations such as the hydrogen binding orientations within the vacancy and where the hole(s) localize. As for the excitation channel at 4.7 eV (SI Figure S11), this could be potentially related to the presence of a larger concentration of H_{O6} defects.

Considering these facts, we present a plausible comprehensive explanation of our experimental findings based on the presented calculations and prior knowledge in β-Ga_2O_3 as follows. Both cation vacancy concentrations and H-levels are likely to be different in as-deposited MOVPE and MBE κ-Ga_2O_3 layers. A plausible assumption is that more V_{Ga} and V_{Ga}-nH deep levels, as well as H_i and H_O shallow donors are present in the as deposited MOVPE material. We can speculate this to be related to an O-richer deposition environment with larger H-contaminations in MOVPE with respect to MEXCAT-MBE. In this regard we cannot exclude a different level of C in the layers, which could be relevant in the suggested picture. The different V_{Ga}-related defects in the as-deposited layers respond strongly to annealing environments at the studied annealing temperatures (*i.e.*, 500 °C).

Differently from the β polymorph, an O_2 annealing at relatively mild temperatures like the ones investigated in this work could redistribute and dissociate various V_{Ga}-nH and H_O populations in κ-Ga_2O_3 (Fig. 9), likely promoting at this stage H_i desorption from the layers [85]. This would result in a more resistive material and influence the population of deep level defects. This effect upon O_2 annealing is much more pronounced in the layers deposited by MOVPE for the different initial content of H and V_{Ga}. In this framework, deep acceptors with different charge states and configurations (*e.g.*, V_{Ga}, V^i_{Ga}, V_{Ga}-nH, Figs. 7 and 8) are generally characterized by different lattice distortions around the defects, which can lead to different emission and capture rates of carriers, with effects on response time to light variation and features of the spectral responsivity in the PDs [86]. The simple variation of the charge state of multivalent acceptor defects in β-Ga_2O_3 has been already demonstrated to induce variations in the hole capture rates [87]. Consistent with the depicted picture, H_2-annealing could passivate (or further passivate) existing V_{Ga} and V_O (and possibly other residual defects – *e.g.*, C-related defects), as well as increase the concentration of H_i in κ-Ga_2O_3. Indeed, this results in a larger conductivity of the material (*i.e.*, larger I_{Dark} in PD) and influence the populations of midgap level defects possibly altering the responsivity under the gap of PDs (Fig. 2).

Again, we highlight that the vertically oriented structural defects of the investigated κ-Ga_2O_3 epitaxial layers may play a critical role in terms of point defects concentration/distribution as well as diffusion channels.

3. Conclusion

This comprehensive study combines extensive experimental and theoretical investigations of the κ-Ga_2O_3 material system and in particular on the role of H-related defects on its functional properties. This is found to have immediate implications for the fabrication of solar-blind UVC photodetectors. Particularly, it is here demonstrated on κ-Ga_2O_3 heteroepitaxial layers deposited with two technologically relevant deposition techniques (MOVPE and MBE) that it is possible to control the concentration of H-related defects through mild annealing treatments with proper background atmosphere. Calculations based on hybrid functionals identify that H can behave in different ways depending on the other defects present in the material, acting as a shallow donor as an interstitial or most substitutional H_O sites, while it can contribute to acceptor concentrations through interactions with V_{Ga} and the most favorable V_O site. In particular, both shallow donors (*e.g.*, H_i) as well as deep acceptors (*e.g.*, V_{Ga}-H complexes) populations can be affected at temperatures significantly lower with respect to the β-Ga_2O_3 polymorph. Additional measurements on how the processing environment influences PD responsivity and the optical signatures associated with deep levels support predictions that hydrogenated vacancy complexes are strongly connected with the resulting PD performance. These experimental findings are an important step further in the physical understanding of these material system and are potentially of great interest for PDs as well as different application fields suggested for the κ-Ga_2O_3 polymorph (*e.g.*, high electron mobility transistors, ferroelectric memory devices).

CRediT authorship contribution statement

P. Mazzolini: Writing – review & editing, Writing – original draft, Visualization, Validation, Supervision, Resources, Project administration, Methodology, Investigation, Funding acquisition, Formal analysis, Data curation, Conceptualization. **J.B. Varley:** Writing – review & editing, Writing – original draft, Visualization, Validation, Resources, Methodology, Investigation, Data curation. **A. Parisini:** Writing – review & editing, Validation, Resources, Methodology, Funding acquisition, Formal analysis. **A. Sacchi:** Visualization, Investigation, Formal analysis, Data curation. **M. Pavesi:** Writing – review & editing, Validation, Resources, Methodology, Formal analysis, Data curation. **A. Bosio:** Resources, Investigation. **M. Bosi:** Writing – review & editing, Validation, Investigation. **L. Seravalli:** Writing – review & editing, Validation, Investigation. **B.M. Janzen:** Validation, Methodology, Investigation, Formal analysis, Data curation. **M.N. Marggraf:** Visualization, Investigation. **N. Bernhardt:** Visualization, Investigation. **M.R. Wagner:** Writing – review & editing, Writing – original draft, Visualization, Validation, Supervision, Resources, Investigation, Formal analysis, Data curation. **A. Ardenghi:** Writing – original draft, Visualization, Investigation, Data curation. **O. Bierwagen:** Writing – review & editing, Validation, Supervision, Resources, Project administration, Funding acquisition. **A. Falkenstein:** Investigation, Data curation. **J. Kler:** Validation, Investigation. **R.A. De Souza:** Writing – review & editing, Writing – original draft, Validation, Supervision, Resources, Investigation, Funding acquisition, Formal analysis, Data curation. **M. Martin:** Writing – review & editing, Validation, Supervision, Resources, Formal

analysis. **F. Mezzadri:** Writing – review & editing, Validation, Investigation. **C. Borelli:** Investigation. **R. Fornari:** Writing – review & editing, Resources, Funding acquisition.

Declaration of competing interest

The authors declare that they have no known competing financial interests or personal relationships that could have appeared to influence the work reported in this paper.

Data availability

Data will be made available on request.

Acknowledgements

The authors would like to thank Ymir Frodason, Beall Fowler, Stephen J. Pearton for fruitful scientific discussion as well as Salvatore Vantaggio for technical assistance. The work by JBV was partially performed under the auspices of the United States Department of Energy (USDOE) by Lawrence Livermore National Laboratory (LLNL) under contract DE-AC52-07NA27344 and partially supported by LLNL Laboratory Directed Research and Development (LDRD) funding under project number 22-SI-003 and by the Critical Materials Institute, an Energy Innovation Hub funded by the USDOE, Office of Energy Efficiency and Renewable Energy, Advanced Manufacturing Office. The MOVPE epitaxial growth of Ga_2O_3 is supported by National Recovery and Resilience Plan (NRRP), Mission 4 Component 2 Investment 1.5 - Call for tender No. 3277 of 30/12/2021 of Italian Ministry of University and Research funded by the European Union – NextGeneration EU, Project "Ecosystem for Sustainable Transition in Emilia-Romagna" (Ecosister, ECS00000033, CUP D93C22000460001). The work at University of Parma has been also financially supported by the project "Ga_2O_3-based diodes for power electronics" (CUP D91B21005370003) through the program FIL 2021, and benefited from the equipment and framework of the COMP-HUB Initiative, funded by the 'Departments of Excellence' program of the Italian Ministry for Education, University and Research (MUR, 2018–2022). The work at Paul Drude Institute was performed in the framework of GraFOx, a Leibniz-ScienceCampus, and was funded by Deutsche Forschungsgemeinschaft (DFG, German Research Foundation) — Project No. 446185170.

Appendix A. Supplementary data

Supplementary data to this article can be found online at https://doi.org/10.1016/j.mtphys.2024.101463.

References

[1] I. Cora, F. Mezzadri, F. Boschi, M. Čaplovičová, G. Calestani, I. Dódony, B. Pécz, R. Fornari, The real structure of ε-Ga2O3 and its relation to κ-phase, CrystEngComm 19 (11) (2017) 1509–1516.

[2] L.E. Ratcliff, T. Oshima, F. Nippert, B.M. Janzen, E. Kluth, R. Goldhahn, M. Feneberg, P. Mazzolini, O. Bierwagen, C. Wouters, M. Nofal, M. Albrecht, J.E. N. Swallow, L.A.H. Jones, P.K. Thakur, T. Lee, C. Kalha, C. Schlueter, T.D. Veal, J. B. Varley, M.R. Wagner, A. Regoutz, "Tackling Disorder in γ-Ga 2 O 3,", Adv. Mater. (2022): 2204217.

[3] R. Roy, V.G. Hill, E.F. Osborn, Polymorphism of Ga2O3 and the system Ga2O3—H2O, J. Am. Chem. Soc. 74 (3) (1952) 719–722.

[4] Z. Galazka, R. Uecker, K. Irmscher, M. Albrecht, D. Klimm, M. Pietsch, M. Brützam, R. Bertram, S. Ganschow, R. Fornari, "Czochralski growth and characterization of β-Ga2O3 single crystals,", Cryst. Res. Technol. 45 (12) (2010) 1229–1236.

[5] S.J. Pearton, J. Yang, P.H. Cary, F. Ren, J. Kim, M.J. Tadjer, M.A. Mastro, A review of Ga2O3 materials, processing, and devices, Appl. Phys. Rev. 5 (1) (2018): 011301.

[6] M. Higashiwaki, K. Sasaki, A. Kuramata, T. Masui, S. Yamakoshi, Gallium oxide (Ga2O3) metal-semiconductor field-effect transistors on single-crystal β-Ga2O3 (010) substrates, Appl. Phys. Lett. 100 (1) (2012): 013504.

[7] A.J. Green, J. Speck, G. Xing, P. Moens, F. Allerstam, K. Gumaelius, T. Neyer, A. Arias-Purdue, V. Mehrotra, A. Kuramata, K. Sasaki, S. Watanabe, K. Koshi, J. Blevins, O. Bierwagen, S. Krishnamoorthy, K. Leedy, A.R. Arehart, A.T. Neal, S. Mou, S.A. Ringel, A. Kumar, A. Sharma, K. Ghosh, U. Singisetti, W. Li, K. Chabak, K. Liddy, A. Islam, S. Rajan, S. Graham, S. Choi, Z. Cheng, M. Higashiwaki, β-Gallium oxide power electronics, Apl. Mater. 10 (2) (2022): 029201.

[8] Y. Kokubun, K. Miura, F. Endo, S. Nakagomi, Sol-gel prepared β-Ga2O3 thin films for ultraviolet photodetectors, Appl. Phys. Lett. 90 (3) (2007): 031912.

[9] X. Arrateig, D. Rogers, P. Maso, F. Bouyssou, I. Sidi-Boumeddine, W. El-Huni, H. Bouhnane, Y. Sama, P. Bove, S. Le Gall, A. Brezart-Oudot, H. Ghorbel, P. Gilbert, V. Sandana, F. Teherani, S. Gautier, A. Darga, Z. Djebbour, A. Ougazzaden, Development and simulated environment testing of β-(Al)Ga2O3-based photodetectors for space-based observation of the Herzberg continuum, in: S. P. Neeck, T. Kimura, S.R. Babu, A. Hélière (Eds.), Sens. Syst. -Gener. Satell. XXV, 2021, p. 41 (SPIE, Online Only, Spain.

[10] N.H. Al-Hardan, M.A. Abdul Hamid, A. Jalar, M. Firdaus-Raih, Unleashing the potential of gallium oxide: a paradigm shift in optoelectronic applications for image sensing and neuromorphic computing applications, Mater. Today Phys. 38 (2023): 101279.

[11] M. Bosi, P. Mazzolini, L. Seravalli, R. Fornari, Ga2O3 polymorphs: tailoring the epitaxial growth conditions, J. Mater. Chem. C 8 (2020) 10975–10992.

[12] M.B. Maccioni, V. Fiorentini, Phase diagram and polarization of stable phases of (Ga1−xInx)2O3, Appl. Phys. Express 9 (4) (2016): 041102.

[13] J. Kim, D. Tahara, Y. Miura, B.G. Kim, First-principle calculations of electronic structures and polar properties of (κ,ε)-Ga2O3, Appl. Phys. Express 11 (6) (2018): 061101.

[14] K. Shimada, First-principles study of crystal structure, elastic stiffness constants, piezoelectric constants, and spontaneous polarization of orthorhombic Pna 2 1 -M 2 O 3 (M = Al, Ga, in: Y. Sc (Ed.), Mater. Res. Express 5 (3) (2018): 036502.

[15] S.B. Cho, R. Mishra, Epitaxial engineering of polar ε-Ga2O3 for tunable two-dimensional electron gas at the heterointerface, Appl. Phys. Lett. 112 (16) (2018): 162101.

[16] P. Ranga, S.B. Cho, R. Mishra, S. Krishnamoorthy, Highly tunable, polarization-engineered two-dimensional electron gas in ε-AlGaO3/ε-Ga2O3 heterostructures, Appl. Phys. Express 13 (6) (2020): 061009.

[17] J. Wang, H. Guo, C.-Z. Zhu, Q. Cai, G.-F. Yang, J.-J. Xue, D.-J. Chen, Y. Tong, B. Liu, H. Lu, R. Zhang, Y.-D. Zheng, ε-Ga2O3: A Promising Candidate for High-Electron-Mobility Transistors, IEEE Electron Device Lett., 2020, 1–1.

[18] F. Mezzadri, G. Calestani, F. Boschi, D. Delmonte, M. Bosi, R. Fornari, Crystal structure and ferroelectric properties of ε-Ga2O3 films grown on (0001)-sapphire, Inorg. Chem. 55 (22) (2016) 12079–12084.

[19] M. Kneiß, P. Storm, A. Hassa, D. Splith, H. von Wenckstern, M. Lorenz, M. Grundmann, Epitaxial growth of κ-(AlxGa1−x)2O3 layers and Superlattice heterostructures up to x = 0.48 on highly conductive Al-doped ZnO thin-film templates by Pulsed Laser deposition, Phys. Status Solidi B n/ a (n/a) (2020): 2000359.

[20] T. Schultz, M. Kneiß, P. Storm, D. Splith, H. von Wenckstern, M. Grundmann, N. Koch, Band Offsets at κ-([Al,In]xGa1–x)2O3/MgO Interfaces, ACS Appl. Mater. Interfaces 12 (7) (2020) 8879–8885.

[21] S. Yusa, D. Oka, T. Fukumura, High- κ dielectric ε-Ga 2 O 3 stabilized in a transparent heteroepitaxial structure grown by mist CVD at atmospheric pressure, CrystEngComm 22 (2) (2020) 381–385.

[22] H.Y. Kang, M.J. Yeom, J.Y. Yang, Y. Choi, J. Lee, C. Park, G. Yoo, R.B. Kyu Chung, Epitaxial κ-Ga2O3/GaN heterostructure for high electron-mobility transistors, Mater. Today Phys. 31 (2023): 101002.

[23] S. Leone, R. Fornari, M. Bosi, V. Montedoro, L. Kirste, P. Doering, F. Benkhelifa, M. Prescher, C. Manz, V. Polyakov, O. Ambacher, Epitaxial growth of GaN/Ga2O3 and Ga2O3/GaN heterostructures for novel high electron mobility transistors, J. Cryst. Growth 534 (2020): 125511.

[24] Y. Kuang, X. Chen, T. Ma, Q. Du, Y. Zhang, J. Hao, F.-F. Ren, B. Liu, S. Zhu, S. Gu, R. Zhang, Y. Zheng, J. Ye, Band Alignment and enhanced Interfacial conductivity Manipulated by polarization in a Surfactant-mediated grown κ-Ga2O3/In2O3 heterostructure, ACS Appl. Electron. Mater. 3 (2) (2021) 795–803.

[25] T. Schultz, M. Kneiß, P. Storm, D. Splith, H. Von Wenckstern, C.T. Koch, A. Hammud, M. Grundmann, N. Koch, Growth of κ-([Al,in] x Ga 1-x) 2 O 3 quantum wells and their potential for quantum-well infrared photodetectors, ACS Appl. Mater. Interfaces 15 (24) (2023) 29535–29541.

[26] P. Mazzolini, Z. Fogarassy, A. Parisini, F. Mezzadri, D. Diercks, M. Bosi, L. Seravalli, A. Sacchi, G. Spaggiari, D. Bersani, O. Bierwagen, B.M. Janzen, M. N. Marggraf, M.R. Wagner, I. Cora, B. Pécz, A. Tahraoui, A. Bosio, C. Borelli, S. Leone, R. Fornari, "Silane-Mediated expansion of domains in Si-doped κ-Ga 2 O 3 epitaxy and its impact on the in-plane electronic conduction,", Adv. Funct. Mater. 33 (2) (2023): 2207821.

[27] Y. Oshima, K. Kawara, T. Oshima, T. Shinohe, In-plane orientation control of (001) κ -Ga 2 O 3 by epitaxial lateral overgrowth through a geometrical natural selection mechanism, Jpn. J. Appl. Phys. 59 (11) (2020): 115501.

[28] V.I. Nikolaev, A.Y. Polyakov, A.V. Myasoedov, I.S. Pavlov, A.V. Morozov, A. I. Pechnikov, I.-H. Lee, E.B. Yakimov, A.A. Vasilev, M.P. Scheglov, A.I. Kochkova, S.J. Pearton, Editors' choice—structural, electrical, and luminescent properties of orthorhombic κ-Ga 2 O 3 grown by epitaxial lateral overgrowth, ECS J. Solid State Sci. Technol. 12 (11) (2023): 115001.

[29] H. Nishinaka, O. Ueda, D. Tahara, Y. Ito, N. Ikenaga, N. Hasuike, M. Yoshimoto, Single-domain and atomically flat surface of κ-Ga2O3 thin films on FZ-grown ε-GaFeO3 substrates via step-flow growth mode, ACS Omega 5 (2020): 29585.

[30] A. Parisini, A. Bosio, H.J. von Bardeleben, J. Jimenez, S. Dadgostar, M. Pavesi, A. Baraldi, S. Vantaggio, R. Fornari, Deep and shallow electronic states associated to doping, contamination and intrinsic defects in ε-Ga2O3 epilayers, Mater. Sci. Semicond. Process. 138 (2022): 106307.

[31] M. Pavesi, F. Fabbri, F. Boschi, G. Piacentini, A. Baraldi, M. Bosi, E. Gombia, A. Parisini, R. Fornari, ε-Ga2O3 epilayers as a material for solar-blind UV photodetectors, Mater. Chem. Phys. 205 (2018) 502–507.

[32] C. Borelli, A. Bosio, A. Parisini, M. Pavesi, S. Vantaggio, R. Fornari, Electronic properties and photo-gain of UV-C photodetectors based on high-resistivity orthorhombic κ-Ga2O3 epilayers, Mater. Sci. Eng. B 286 (2022): 116056.

[33] D. Kaur, M. Kumar, A strategic review on gallium oxide based deep-ultraviolet photodetectors: recent progress and future prospects, Adv. Opt. Mater. 9 (9) (2021): 2002160.

[34] P. Weiser, M. Stavola, W.B. Fowler, Y. Qin, S. Pearton, Structure and vibrational properties of the dominant O-H center in β-Ga2O3, Appl. Phys. Lett. 112 (23) (2018): 232104.

[35] W.B. Fowler, M. Stavola, Y. Qin, P. Weiser, Trapping of multiple H atoms at the Ga (1) vacancy in β-Ga2O3, Appl. Phys. Lett. 117 (14) (2020): 142101.

[36] Y. Qin, M. Stavola, W.B. Fowler, P. Weiser, S.J. Pearton, Hydrogen centers in β-Ga2O3: infrared spectroscopy and density functional theory, ECS J. Solid State Sci. Technol. 8 (7) (2019) Q3103–Q3110.

[37] V.M. Reinertsen, P.M. Weiser, Y.K. Frodason, M.E. Bathen, L. Vines, K. M. Johansen, Anisotropic and trap-limited diffusion of hydrogen/deuterium in monoclinic gallium oxide single crystals, Appl. Phys. Lett. 117 (23) (2020): 232106.

[38] P.D.C. King, I. McKenzie, T.D. Veal, Observation of shallow-donor muonium in Ga2O3: evidence for hydrogen-induced conductivity, Appl. Phys. Lett. 96 (6) (2010): 062110.

[39] O. Bierwagen, P. Vogt, P. Mazzolini, Plasma-assisted molecular beam epitaxy 2, in: M. Higashiwaki, S. Fujita (Eds.), Gallium Oxide Mater. Prop. Cryst. Growth Devices, Springer International Publishing, Cham, 2020, pp. 95–121.

[40] P. Vogt, O. Brandt, H. Riechert, J. Lähnemann, O. Bierwagen, Metal-exchange catalysis in the growth of sesquioxides: towards heterostructures of transparent oxide semiconductors, Phys. Rev. Lett. 119 (19) (2017): 196001.

[41] A. Bosio, C. Borelli, A. Parisini, M. Pavesi, S. Vantaggio, R. Fornari, A metal-oxide contact to ε-Ga2O3 epitaxial films and relevant conduction mechanism, ECS J. Solid State Sci. Technol. 9 (5) (2020): 055002.

[42] J. Heyd, G.E. Scuseria, M. Ernzerhof, Hybrid functionals based on a screened Coulomb potential, J. Chem. Phys. 118 (18) (2003) 8207–8215.

[43] P.E. Blöchl, Projector augmented-wave method, Phys. Rev. B 50 (24) (1994) 17953–17979.

[44] G. Kresse, J. Furthmüller, Efficient iterative schemes for ab initio total-energy calculations using a plane-wave basis set, Phys. Rev. B 54 (16) (1996) 11169–11186.

[45] G. Kresse, J. Furthmüller, Efficiency of ab-initio total energy calculations for metals and semiconductors using a plane-wave basis set, Comput. Mater. Sci. 6 (1) (1996) 15–50.

[46] C. Freysoldt, J. Neugebauer, C.G. Van De Walle, Electrostatic interactions between charged defects in supercells: electrostatic interactions between charged defects in supercells, Phys. Status Solidi B 248 (5) (2011) 1067–1076.

[47] C. Freysoldt, B. Grabowski, T. Hickel, J. Neugebauer, G. Kresse, A. Janotti, C. G. Van De Walle, First-principles calculations for point defects in solids, Rev. Mod. Phys. 86 (1) (2014) 253–305.

[48] A. Jain, S.P. Ong, G. Hautier, W. Chen, W.D. Richards, S. Dacek, S. Cholia, D. Gunter, D. Skinner, G. Ceder, K.A. Persson, Commentary: the Materials Project: a materials genome approach to accelerating materials innovation, Apl. Mater. 1 (1) (2013): 011002.

[49] T. Gake, Y. Kumagai, C. Freysoldt, F. Oba, Finite-size corrections for defect-involving vertical transitions in supercell calculations, Phys. Rev. B 101 (2) (2020): 020102.

[50] A. Alkauskas, M.D. McCluskey, C.G. Van De Walle, Tutorial: defects in semiconductors—combining experiment and theory, J. Appl. Phys. 119 (18) (2016): 181101.

[51] H. Nishinaka, H. Komai, D. Tahara, Y. Arata, M. Yoshimoto, Microstructures and rotational domains in orthorhombic ε-Ga2O3 thin films, Jpn. J. Appl. Phys. 57 (11) (2018): 115601.

[52] J.E.N. Swallow, C. Vorwerk, P. Mazzolini, P. Vogt, O. Bierwagen, A. Karg, M. Eickhoff, J. Schörmann, M.R. Wagner, J.W. Roberts, P.R. Chalker, M.J. Smiles, P. Murgatroyd, S.A. Razek, Z.W. Lebens-Higgins, L.F.J. Piper, L.A.H. Jones, P. K. Thakur, T.-L. Lee, J.B. Varley, J. Furthmüller, C. Draxl, T.D. Veal, A. Regoutz, Influence of polymorphism on the electronic structure of Ga2O3, Chem. Mater. 32 (19) (2020) 8460–8470.

[53] M. Kneiß, A. Hassa, D. Splith, C. Sturm, H. von Wenckstern, M. Lorenz, M. Grundmann, Epitaxial stabilization of single phase κ-(InxGa1−x)2O3 thin films up to x = 0.28 on c-sapphire and κ-Ga2O3(001) templates by tin-assisted VCCS-PLD, Apl. Mater. 7 (10) (2019): 101102.

[54] P. Mazzolini, A. Falkenstein, C. Wouters, R. Schewski, T. Markurt, Z. Galazka, M. Martin, M. Albrecht, O. Bierwagen, Substrate-orientation dependence of β-Ga2O3 (100), (010), (001), and (2¯01) homoepitaxy by indium-mediated metal-exchange catalyzed molecular beam epitaxy (MEXCAT-MBE), Apl. Mater. 8 (1) (2020): 011107.

[55] R. Fornari, M. Pavesi, V. Montedoro, D. Klimm, F. Mezzadri, I. Cora, B. Pécz, F. Boschi, A. Parisini, A. Baraldi, C. Ferrari, E. Gombia, M. Bosi, Thermal stability of ε-Ga2O3 polymorph, Acta Mater. 140 (Supplement C) (2017) 411–416.

[56] Q. Zhang, N. Li, T. Zhang, D. Dong, Y. Yang, Y. Wang, Z. Dong, J. Shen, T. Zhou, Y. Liang, W. Tang, Z. Wu, Y. Zhang, J. Hao, Enhanced gain and detectivity of unipolar barrier solar blind avalanche photodetector via lattice and band engineering, Nat. Commun. 14 (1) (2023) 418.

[57] Y. Wang, S. Li, J. Cao, Y. Jiang, Y. Zhang, W. Tang, Z. Wu, Improved response speed of β-Ga2O3 solar-blind photodetectors by optimizing illumination and bias, Mater. Des. 221 (2022): 110917.

[58] S. Li, J. Yue, X. Ji, C. Lu, Z. Yan, P. Li, D. Guo, Z. Wu, W. Tang, Oxygen vacancies modulating the photodetector performances in ε-Ga2O3 thin films, J. Mater. Chem. C 9 (16) (2021) 5437–5444.

[59] H. Idriss, On the wrong assignment of the XPS O1s signal at 531–532 eV attributed to oxygen vacancies in photo- and electro-catalysts for water splitting and other materials applications, Surf. Sci. 712 (2021): 121894.

[60] J. Stoch, J. Gablankowska-Kukucz, The effect of carbonate contaminations on the XPS O 1s band structure in metal oxides, Surf. Interface Anal. 17 (3) (1991) 165–167.

[61] A. Shchukarev, D. Korolkov, XPS Study of group IA carbonates, Open Chem. 2 (2) (2004) 347–362.

[62] J.E.N. Swallow, J.B. Varley, L.A.H. Jones, J.T. Gibbon, L.F.J. Piper, V.R. Dhanak, T. D. Veal, Transition from electron accumulation to depletion at β-Ga2O3 surfaces: the role of hydrogen and the charge neutrality level, Apl. Mater. 7 (2) (2019): 022528.

[63] A. Karg, M. Kracht, P. Vogt, A. Messow, N. Braud, J. Schörmann, M. Rohnke, J. Janek, J. Falta, M. Eickhoff, Enhanced epitaxial growth of Ga 2 O 3 using an ultrathin SnO 2 layer, J. Appl. Phys. 132 (19) (2022): 195304.

[64] M. Mulazzi, F. Reichmann, A. Becker, W.M. Klesse, P. Alippi, V. Fiorentini, A. Parisini, M. Bosi, R. Fornari, The electronic structure of ε-Ga2O3, Apl. Mater. 7 (2) (2019): 022522.

[65] H.J. von Bardeleben, J.L. Cantin, A. Parisini, A. Bosio, R. Fornari, Conduction mechanism and shallow donor properties in silicon-doped ε -G a 2 O 3 thin films: an electron paramagnetic resonance study, Phys. Rev. Mater. 3 (8) (2019): 084601.

[66] T. Gake, Y. Kumagai, F. Oba, First-principles study of self-trapped holes and acceptor impurities in Ga 2 O 3 polymorphs, Phys. Rev. Mater. 3 (4) (2019): 044603.

[67] V. Montedoro, A. Torres, S. Dadgostar, J. Jimenez, M. Bosi, A. Parisini, R. Fornari, Cathodoluminescence of undoped and Si-doped ε-Ga2O3 films, Mater. Sci. Eng. B 264 (2021): 114918.

[68] B.M. Janzen, P. Mazzolini, R. Gillen, V.F.S. Peltason, L.P. Grote, J. Maultzsch, R. Fornari, O. Bierwagen, M.R. Wagner, Comprehensive Raman study of orthorhombic κ/ε-Ga2O3 and the impact of rotational domains, J. Mater. Chem. C 9 (2021) 14175 - 14189.

[69] S. Seacat, J.L. Lyons, H. Peelaers, Orthorhombic alloys of Ga 2 O 3 and Al 2 O 3, Appl. Phys. Lett. 116 (23) (2020): 232102.

[70] J.B. Varley, J.R. Weber, A. Janotti, C.G. Van de Walle, Oxygen vacancies and donor impurities in β-Ga2O3, Appl. Phys. Lett. 97 (14) (2010): 142106.

[71] A. Karjalainen, V. Prozheeva, K. Simula, I. Makkonen, V. Callewaert, J.B. Varley, F. Tuomisto, Split Ga vacancies and the unusually strong anisotropy of positron annihilation spectra in β − Ga 2 O 3, Phys. Rev. B 102 (19) (2020): 195207.

[72] A. Karjalainen, P.M. Weiser, I. Makkonen, V.M. Reinertsen, L. Vines, F. Tuomisto, Interplay of vacancies, hydrogen, and electrical compensation in irradiated and annealed n -type β -Ga 2 O 3, J. Appl. Phys. 129 (16) (2021): 165702.

[73] F. Tuomisto, Ga vacancies in β-Ga 2 O 3 : split or not? Jpn. J. Appl. Phys. 62 (SF) (2023): SF0802.

[74] A. Karjalainen, I. Makkonen, J. Etula, K. Goto, H. Murakami, Y. Kumagai, F. Tuomisto, Split Ga vacancies in n -type and semi-insulating β-Ga 2 O 3 single crystals, Appl. Phys. Lett. 118 (7) (2021): 072104.

[75] F. Tuomisto, A. Karjalainen, I. Makkonen, Split Ga vacancies: abundant defects in beta-Ga2O3, in: F.H. Teherani, D.C. Look, D.J. Rogers (Eds.), Oxide-Based Mater. Devices XII, SPIE, Online Only, United States, 2021, p. 6.

[76] J.B. Varley, H. Peelaers, A. Janotti, C.G. Van de Walle, Hydrogenated cation vacancies in semiconducting oxides, J. Phys. Condens. Matter 23 (33) (2011): 334212.

[77] Y.K. Frodason, J.B. Varley, K.M.H. Johansen, L. Vines, C.G. Van de Walle, Migration of Ga vacancies and interstitials in β − Ga 2 O 3, Phys. Rev. B 107 (2) (2023): 024109.

[78] Y.K. Frodason, C. Zimmermann, E.F. Verhoeven, P.M. Weiser, L. Vines, J.B. Varley, Multistability of isolated and hydrogenated Ga–O divacancies in β − Ga 2 O 3, Phys. Rev. Mater. 5 (2) (2021): 025402.

[79] S. Mu, M. Wang, J.B. Varley, J.L. Lyons, D. Wickramaratne, C.G. Van De Walle, "Role of carbon and hydrogen in limiting n -type doping of monoclinic (Al x Ga 1 −x) 2 O 3,", Phys. Rev. B 105 (15) (2022): 155201.

[80] P. Rajabi Kalvani, A. Parisini, G. Sozzi, C. Borelli, P. Mazzolini, O. Bierwagen, S. Vantaggio, K. Egbo, M. Bosi, L. Seravalli, R. Fornari, Interfacial properties of the SnO/κ-Ga $_2$ O $_3$ p-n heterojunction: a case of subsurface doping density reduction via thermal treatment in κ-Ga $_2$ O $_3$, ACS Appl. Mater. Interfaces 15 (39) (2023) 45997–46009.

[81] J.M. Johnson, Z. Chen, J.B. Varley, C.M. Jackson, E. Farzana, Z. Zhang, A. R. Arehart, H.-L. Huang, A. Genc, S.A. Ringel, C.G. Van de Walle, D.A. Muller, J. Hwang, Unusual Formation of point-defect complexes in the ultrawide-band-gap semiconductor β − Ga 2 O 3, Phys. Rev. X 9 (4) (2019): 041027.

[82] J.B. Varley, A. Janotti, C. Franchini, C.G. Van de Walle, Role of self-trapping in luminescence and p -type conductivity of wide-band-gap oxides, Phys. Rev. B 85 (8) (2012): 081109.

[83] J.L. Lyons, Electronic properties of Ga $_2$ O $_3$ polymorphs, ECS J. Solid State Sci. Technol. 8 (7) (2019) Q3226–Q3228.

[84] S. Marcinkevičius, J.S. Speck, Ultrafast dynamics of hole self-localization in *β* -Ga2O3, Appl. Phys. Lett. 116 (13) (2020): 132101.

[85] A. Goyal, A. Zakutayev, V. Stevanović, S. Lany, Computational Fermi level engineering and doping-type conversion of Mg:Ga2O3 via three-step synthesis process, J. Appl. Phys. 129 (24) (2021): 245704.
[86] J. Bourgoin, M. Lannoo, G.D. Watkins, Point Defects in Semiconductors, Springer-Verlag, Berlin Heidelberg New York, 1983.
[87] Y. Fang, J. Wang, F. Shi, Z. Xiao, X. Wu, J. Yang, Y. Chen, Q. Wu, Y. Song, Native defect-related broadband ultrafast photocarrier dynamics in n-type β -Ga2O3, Appl. Phys. Lett. 121 (11) (2022): 112103.